Ab initio chemical kinetics for the HCCO+OH reaction

ARTICLE *in* CHEMICAL PHYSICS LETTERS · JANUARY 2014

Impact Factor: 1.9 · DOI: 10.1016/j.cplett.2013.11.060

6 AUTHORS, INCLUDING:

Tam Mai
Institute for Computational Science and Te…
8 PUBLICATIONS **6** CITATIONS
SEE PROFILE

Xuan T. Le
Institute for Computational Science and Te…
7 PUBLICATIONS **6** CITATIONS
SEE PROFILE

Lam Huynh
Vietnam National University, Ho Chi Minh City
40 PUBLICATIONS **583** CITATIONS
SEE PROFILE

Pham Cam Nam
The University of Da Nang -University of Sci…
13 PUBLICATIONS **74** CITATIONS
SEE PROFILE

Chemical Physics Letters 592 (2014) 175–181

Contents lists available at ScienceDirect

Chemical Physics Letters

journal homepage: www.elsevier.com/locate/cplett

Ab initio chemical kinetics for the HCCO + OH reaction

Tam V.-T. Mai [a], P. Raghunath [b], Xuan T. Le [a], Lam K. Huynh [a,*], Pham-Cam Nam [c,1], M.C. Lin [b,d,*]

[a] Institute for Computational Science and Technology and International University, Vietnam National University, Ho Chi Minh City, Viet Nam
[b] Center for Interdisciplinary Molecular Science, Department of Applied Chemistry, Hsinchu 300, Taiwan
[c] Danang University of Science Technology, The University of Danang, Viet Nam
[d] Department of Chemistry, Emory University, Atlanta, GA, USA

ARTICLE INFO

Article history:
Received 4 October 2013
In final form 29 November 2013
Available online 8 December 2013

ABSTRACT

The mechanism for the reaction of HCCO and OH has been investigated at different high-levels of theory. The reaction was found to occur on singlet and triplet potential energy surfaces with multiple accessible paths. Rate constants predicted by variational RRKM/ME calculations show that the reaction on both surfaces occurs primarily by barrierless OH attack at both C atoms producing excited intermediates which fragment to produce predominantly CO and ^{1,3}HCOH with $k_S = 3.12 \times 10^{-8}\ T^{-0.59}\exp[-73.0/T]$ and $k_T = 6.29 \times 10^{-11}\ T^{0.13}\exp[108/T]$ cm^3 molecule^{-1} s^{-1} at $T = 300$–2000 K, independent of pressure at $P < 76\,000$ Torr.

1. Introduction

The ketenyl (HCCO) radical has been considered as a key intermediate in the oxidation of hydrocarbon fuels, especially in the case of acetylene, an important core hydrocarbon and also a major intermediate in almost all hydrocarbon-fueled flames. Ketenyl is mainly formed by the $C_2H_2 + O$ reaction [1–5] whose two important product channels are:

$$C_2H_2 + O(^3P) \rightarrow HCCO + H \qquad \text{(Rxn.1)}$$

$$\rightarrow CH_2 + CO \qquad \text{(Rxn.2)}$$

where HCCO is found to be the principal product accounting for more than 60% of product yield in a wide range of temperature and pressure. Therefore, subsequent ketenyl consumption has attracted much attention. Specifically, there are a number of experimental as well as theoretical studies on the reactions of HCCO with other species such as H [2,6], O[7–9], O_2[10–14], H_2[15], C_2H_2 [11,14,16], NO [14,17–21], NO_2 [14,15,22–24] and SO_2 [25].

Of the most reactive species, especially in the combustion of hydrocarbons, OH radical plays the most important role in the ketenyl oxidation chemistry. However, not much reliable and comprehensive kinetic information, both theoretically and experimentally, is available for the reaction of HCCO and OH, except estimated rate constants for direct hydrogen abstraction which have been included inconsistently in available kinetic models (e.g., OH + HCCO → $C_2O + H_2O$ [26], OH + HCCO → H_2CCO + O [26,27], OH + HCCO → HCCOH + O [27]), in order to fit simulation species profiles to experimental data under different conditions. This is our motivation to accurately characterize the kinetic behaviors of the reaction.

The HCCO + OH reaction can proceed by either addition of the OH to the C=C Π-bond of HCCO at two different C-sites to form energized adducts, followed by their unimolecular reactions, or by direct mutual hydrogen abstraction reactions. These reactions can occur on both singlet and triplet surfaces consisting of multiple wells (intermediates) via multiple paths. Therefore, in this Letter, the potential energy surfaces (PES's) of the HCCO + OH reaction have been explored using highly accurate levels of theory, such as CBS-QB3, CBS-APNO and W1U. On such well-characterized PES's, rate constant calculations for all accessible channels are then carried out to identify the formation of major products as well as their branching ratios under different conditions of temperatures and pressures of relevance to combustion. Thermodynamic data for all related species are also derived so that the detailed kinetics for the HCCO + OH sub-mechanism can be used as a core sub-model for construction of detailed oxidation mechanisms of real fuels.

2. Computational methods

2.1. Electronic structure calculations

All calculations were carried out using the Gaussian09 [28] program. The composite CBS-QB3 method by Peterson and coworkers [29] was employed as an effective compromising method in terms of accuracy and computational time. The highly-accurate methods,

* Corresponding authors at: International University, Vietnam National University, Ho Chi Minh City, Viet Nam (L.K.H.) and Center for Interdisciplinary Molecular Science, Department of Applied Chemistry, Hsinchu, Taiwan (M.C. Lin).
E-mail addresses: hklam@hcmiu.edu.vn (L.K. Huynh), chemmcl@emory.edu (M.C. Lin).
[1] Emerson Visiting Fellow, Dec. 2009–Apr. 2010.

0009-2614/$ - see front matter © 2013 Elsevier B.V. All rights reserved.
http://dx.doi.org/10.1016/j.cplett.2013.11.060

namely CBS-APNO [30] and W1U [31], were also utilized as a reference point for the CBS-QB3 calculations. All reported results for stable molecules as well as transition states were obtained for the lowest-lying conformer of a given species.

For barrierless reactions occurring without intrinsic transition states, conventional single-reference methods might fail to accurately capture the potential surface when the fragments are farther away. For this reason, the multi-reference CASPT2 method [32] was used to characterize such channels. All of these calculations were carried out using the Molpro2010 [33] program.

2.2. Rate constant calculations

Temperature- and pressure-dependent rate constants for key low-lying reaction channels on the PES's have been calculated using Rice–Ramsperger–Kassel–Marcus-based Master Equation (RRKM/ME) methodology implemented in the Variflex code [34]. For barrierless channels, we did variationally the optimized bond length to separated radical pairs with an interval of 0.1 Å by second-order multireference perturbation theory CASPT2(12e,9o)//CAS(12e,9o) method with cc-pVTZ and 6−311 + G(3df,p) basis sets. The discrete CASPT2 values were fitted to a Morse potentialby which the rate constants were derived. Lennard–Jones (LJ) parameters, σ = 3.47 Å and ε/k_B = 114 K for Ar bath gas was taken from the literature [35] while the values σ = 4.41 and ε/k_B = 470 K were estimated based on similar species (e.g., $C_2H_5O_2$ from LLNL mechanisms [36]).The energy transfer per downward collision was approximated using the exponential down model with $\langle \Delta E_{down} \rangle = 400\ cm^{-1}$. Hindered internal rotation (HIR) and Eckart tunneling corrections were included.

3. Results and discussion

3.1. Potential energy surface and reaction mechanism

In order to characterize the kinetics of the reaction between HCCO and OH, a reliable and detailed PES is needed. To our best knowledge, such a PES is not available for this system; thus we have attempted to construct it using high levels of theory. Figure 1 presents the PES at 0 K of the HCCO–OH system established by the composite CBS-QB3 method. For clarity, high-energy reaction channels having barriers higher than 65 kcal/mol above the entrance level, such as CHCOOH (IM9) → products, are not included. In addition, values obtained by other highly accurate methods (W1U and CBS-APNO), are given in Supplementary Table S2. Optimized geometries of all species with important geometrical parameters at the CBS-QB3 level are provided in Supplementary Figure S1. Detailed molecular information of the involved species can be found in Supplementary Table S4. To facilitate the discussion, the CBS-QB3 values are used universally and the energies are cited relative to that of the reactants; otherwise it will be explicitly stated.

3.1.1. Singlet sub-surface

Figure 1a presents the singlet sub-surface of the HCCO and OH reaction forming internally-energized adducts by C—O bond formation. The hydroxyl radical can add to one of the two C atoms of HCCO to form either hydroxyl ketene, HOCH=C=O (**IM1**), or carboxyl methylidene, HC=C(=O)OH (**IM4**), occurring barrierlessly with high exothermicity (ΔH_{rxn} (0 K = −87.1 and −44.0 kcal/mol, respectively). The energized adducts can undergo reactions by isomerization and dissociation, and by collisional deactivation. These competing processes will change product branching ratios with temperature and pressure.

From the more stable adduct **IM1**, 9 possible reaction pathways can occur as described below:

(1) *HCCO + OH (**R**) redissociation*. The adduct **IM1** can redissociate back to the reactants along the minimum energy path (MEP) characterized by variable reaction coordinate transition state theory (VRC-TST).
(2) *H_2CO + CO (**P2**) formation*. This is the second most thermodynamically favorable channel whose products are formed via the 1,2-H-shift across the C—O bond, accompanied by the C=C bond breaking. This channel has the barrier energy of 60.3 kcal/mol, lying at −26.8 kcal/mol; thus this channel is expected to be important, especially at low temperatures.
(3) *CO + ^{1}HCOH (**P3**) formation*. The C=C bond at **IM1** can be directly broken to form CO and singlet-state hydroxymethylene ^{1}HCOH with the barrier close to reaction energy (−49.8 and −52.3 kcal/mol, respectively), suggesting that the TS has the product-like structure (cf. Figure S1).
(4) *H + OCHCO (**P6**) formation*. The breaking of the O—H bond to give H + OCHCO (**P6**) with a high barrier of 70.7 kcal/mol but still lying below the entrance channel (−16.4 kcal/mol).
(5) *H + HOCCO (**P9**) formation*. Similar to the previous channel, **IM1** can dissociate to H + HOCCO by breaking the C—H bond. Due to missing resonance structure as observed in **P6** (O*—CH=C=O ↔ O=CH—C*=O forms), this channel has a higher barrier (92.3 vs. 70.7 kcal/mol).
(6) *H_2O + ^{1}CCO (**P8**) formation*. These bimolecular products can be formed via the van der Waals complex (**C1**) whose barrier (from **IM1**) and energy is 9.3 and 17.8 kcal/mol below the entrance channel, respectively. It is expected that a roaming TS can exist between the reactants and these products; however, because the energy of H_2O + ^{1}CCO is comparable with the reactant energy (0.1 kcal/mol above the reactants), the formation via such a TS is expected to play a less important role comparing to the other low-energy lying channels.
(7) *trans-glyoxal (IM2) isomerization and subsequent reactions*. Hydrogen of the OH group can undergo a 1,3-H migration to form *trans*-glyoxal (**IM2**) with a barrier height of 55.8 kcal/mol and reaction energy of −15.4 kcal/mol. Intermediate **IM2** then can either dissociate to form CO + H_2CO (**P2**), CO + ^{1}HCOH (**P3**), CHO + CHO (**P5**) or isomerize to *cis*-glyoxal (**IM3**) which can subsequently dissociate to 2CO + H_2 (**P1**), the most thermodynamically favorable products (−107.7 kcal/mol).
(8) *^{1}CH=C(=O)OH (**IM4**) isomerization*. Singlet-state carboxyl methylidene can be formed through the OH migration from IM1 to the C atom of the carbonyl group with a barrier energy of 49.2 kcal/mol. Alternatively, the adduct can be formed directly from the addition of OH to carbonyl carbon of HCCO. The **IM1**–**IM4** connection makes the potential more complicated especially in kinetic analysis.
(9) *HC≡COOH (**IM9**) isomerization*. The rearrangement to the peroxy compound HC≡C—OOH is very tight with a high reaction barrier of 95.4 kcal/mol. The subsequent decomposition reaction of IM9 occurs even with a much higher barrier (e.g., 65 kcal/mol above the entrance channel); thus it is not included in the analysis.

In the same manner, the initially-formed adduct **IM4** can undergo isomerization to form **IM1** and oxiran-2-one (**IM5**) or redissociate back to the reactants, HCCO + OH. Oxiran-2-one then can decompose by simultaneously breaking the C–O and C–C bonds of the oxirane ring to give CO_2 + $^1CH_2$ products (P4). These channels have relative energies much below the reactant energy (−41.7 and −36.7 kcal/mol for **IM4** → **IM5** and **IM5** → P4, respectively); thus they can strongly compete with other channels at low temperature and high pressure.

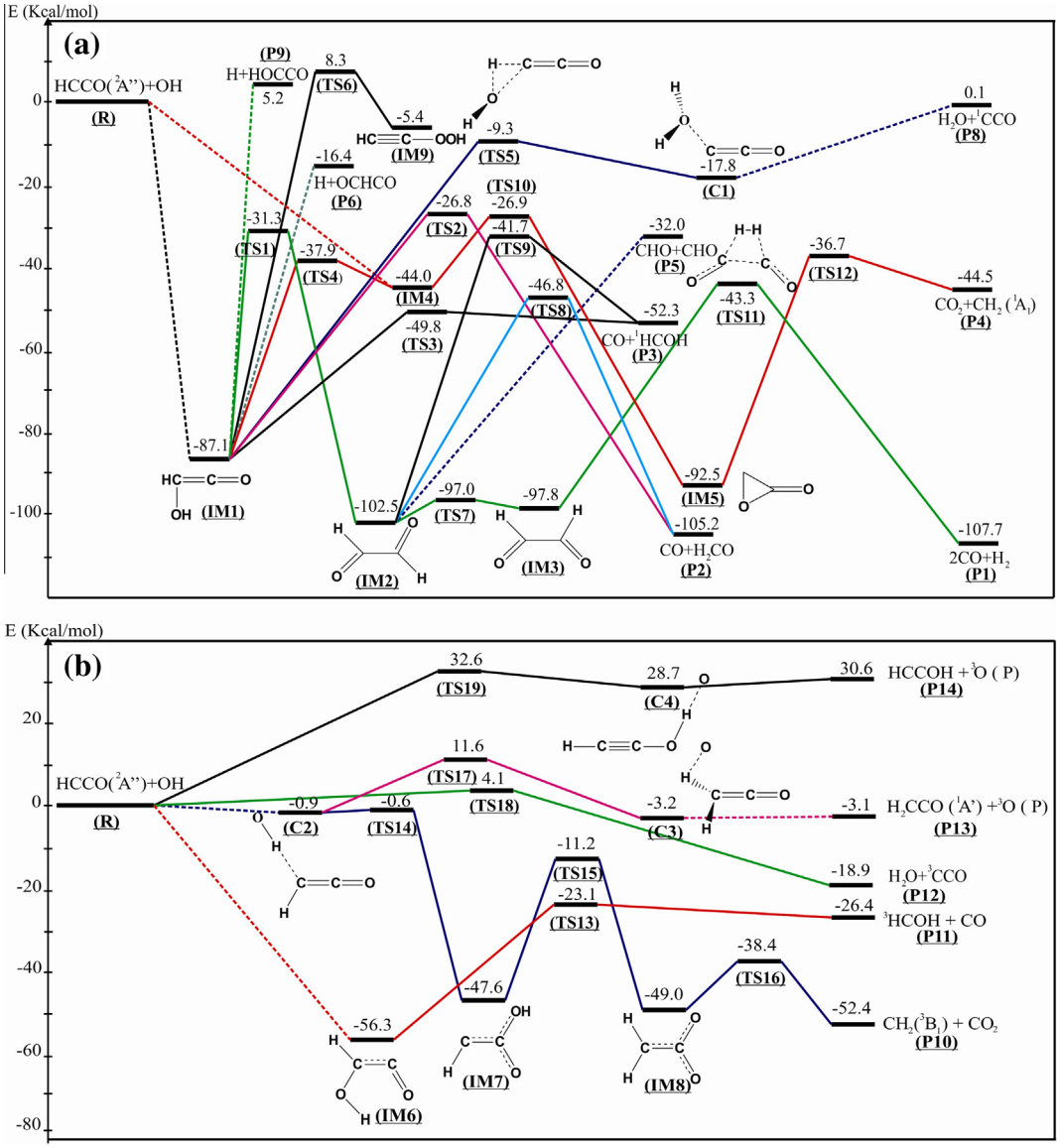

Figure 1. The simplified potential energy surface (0 K) computed at the CBS-QB3 level for possible channels of the HCCO + OH reaction: (a) Singlet and (b) Triplet surfaces. High-energy channels are not included for clarity. Values are in kcal/mol.

3.1.2. Triplet sub-surface

Similarly, on this sub-surface shown in Figure 1b hydroxyl radical can attach to both C atoms of HCCO via complex **C2** to form triplet-state adducts **IM7** and **IM6** with much shallower well-depths. These adducts can isomerize and/or decompose to form bimolecular products. Alternatively, direct hydrogen abstraction channels also exist on this triplet sub-surface to form $H_2O + {}^3CCO$ (P12), $H_2CCO + {}^3O$ (P13) and $HCCOH + {}^3O$ (P14). These channels are described as follows

(1) *$^3CH_2 + CO_2$ (**P10**) formation.* This is the most stable product channel on this subsurface with the relative energy of −52.4 kcal/mol. Initially, the reactant combination results in a van der Waals complex HO...CHCO (C2) which then can transform to $^3CHC(OH)=O$ (**IM7**) through a very loose and low-energy TS with the barrier of 0.3 kcal/mol. The adduct **IM7** can isomerizes through a four-member-ring H-migration TS to form $^3CH_2CO_2$ (**IM8**) before dissociating to the final products, $^3CH_2 + CO_2$, by breaking the C–C bond.

(2) *$^3HCOH + CO$ (**P11**) formation.* The adduct ^{3}HOCHCO (**IM6**) can be formed by OH addition to the H-containing C atom. This process is barrierless with the reaction energy of −56.3 kcal/mol. From this adduct $^3HCOH + CO$ (**P11**) can be formed with a relative energy of −26.4 kcal/mol, having a product-like TS (the reaction barrier and energy are 33.2 and 29.9 kcal/mol, respectively).

(3) *$^3CCO + H_2O$ (**P12**) formation (H-abstraction by OH).* The OH radical can directly abstract H atom of HCCO to form $^3CCO + H_2O$ with the barrier of 4.1 kcal/mol.

(4) *$H_2CCO + {}^3O$ (**P13**) formation (H-abstraction by HCCO).* The H abstraction from OH by the H-containing C atom of HCCO goes through the formation of the complex **C2** before forming $H_2CCO + {}^3O$ products (**P13**). The calculated barrier height for this process is 12.5 kcal/mol at the CBS-QB3 level; the products form a post-reaction van der Waals complex, O...CH_2CO (**C3**), which can easily decompose to the product (at −3.1 kcal/mol) with no TS.

(5) *HC≡COH + ^3O (**P14**) formation (H-abstraction by HCCO).* The O atom of HCCO radical can abstract the H-atom of OH to give

HCCOH + ^{3}O (**P14**) products. This reaction occurs through a tight TS, followed by a van der Waals complex **C4** which is 1.9 kcal/mol below the products. The TS has a relatively high energy of 32.6 kcal/mol via a van der Waals complex C4; this channel is expected to be less favorable than others.

The calculated PES at the CBS-QB3 level agrees very well with the one obtained with the more accurate W1U method, typically within 1 kcal/mol for reaction barriers and reaction energies (c.f. Supplementary Table S2 for details). In this context, the CBS-QB3 values are even better than the CBS-ANPO values. Such an excellent agreement provides us with confidence in using the CSB-QB3 energies for thermodynamic calculations and kinetic analysis.

3.2. Thermodynamic properties calculations

Table 1 presents the calculated reaction enthalpies at different levels of theory in this study, namely CBS-QB3, W1U and CBS-APNO. The CBS-QB3 values are found to be closer to the most accurate W1U results than the CBS-APNO ones. The CBS-QB3 values predicted at 298 K are also provided for comparison with available experimental/ab initio data. Good agreement was achieved typically within 1 kcal/mol.

The reaction barriers for selected reactions at different levels are shown in Table 2. It is worth mentioning that the CBS-QB3 numbers are almost identical to those from W1U which is an expensive method. Thus CBS-QB3 is the method of choice for both accuracy and computational time.

3.2.1. Ketenyl (HCCO) radical

The HCCO radical has been a subject of several experimental and theoretical studies [42–49]. Some basic thermochemical parameters have also been determined by experiments including the heat of formation (ΔH_f) [47], electron affinity (EA) [44,45] and bond dissociation energy (BDE) [44]. Table 3 presents the calculated values in comparison with available data in the literature. Evidently our CBS-QB3 values agree better with the available experimental data.

3.3. Rate constant calculations

Rate constants for all reaction channels on the well-defined PES described in Figure 1 have been predicted by RRKM/ME calculations. The high-pressure limit rate constant for barrier less reactions are computed by using the VRC-TST approach with the CASPT2 potential.

3.3.1. Reactions on the singlet surface

As aforementioned, there are two initial association paths for HCCO + OH, taking place by OH addition to the two different C atoms producing HC(OH)=CO (**IM1**) and HCC(OH)=O (**IM4**) with 87.1 and 44.0 kcal/mol of internal excitation, respectively. **IM4** can isomerize to **IM1** by OH-migration via a small (6.1 kcal/mol) barrier at TS4 because of the instability of the former, carboxyl methylidine. The computed potential energies for **IM1** and **IM4** decomposition to HCCO + OH along their barrierless MEP's could be fitted to the Morse function with $\beta = 2.41$ Å^{-1} and $\beta = 2.02$ Å^{-1}, respectively; these values were used for C–O bond breaking rate constant calculations. The high pressure-limit rate constants for the initial association processes predicted for two temperature ranges based on the computed VTS curves by CASPT2 can be represented by the following equations in units of cm^3 molecule^{-1} s^{-1}:

$$k^{\infty}_{R\rightarrow IM1} = 2.54\times10^{-10}\exp[-57.1/T]\ (300-1000\ \mathrm{K}) \quad \text{(Eq.2a)}$$

$$= 6.16\times10^{-11}T^{0.19}\exp[42.4/T]\ (300-2000\ \mathrm{K}) \quad \text{(Eq.2b)}$$

$$k^{\infty}_{R\rightarrow IM4} = 2.45\times10^{-10}\exp[-40.7/T]\ (300-1000\ \mathrm{K}) \quad \text{(Eq.3a)}$$

$$= 8.40\times10^{-11}T^{0.14}\exp[34.5/T]\ (300-2000\ \mathrm{K}) \quad \text{(Eq.3b)}$$

Both rate constants appear to be very similar in magnitude (as can be more clearly seen from their Arrhenius expressions derived for the low-T range, Eqs. 2a and 3a, reflecting the close similarity in the two variational association processes. We have done the rate constant calculations using the W1U energies for the forward reactions of HCCO + OH via singlet and triplet surface producing various low energy products with multiple reflection corrections and compared with those by CBS-QB3 are shown in Supplementary Figures S3 and S4. All the calculations at the W1U level of theory are in good agreement with those by the CBS-QB3 method. Under practical T, P-conditions, the internally-excited adducts can readily undergo isomerization and fragmentation producing various products; these reactions are competitive with the collisional quenching process which gives rise to the pressure dependence. The specific rate constants for the isomerization and decomposition of the two excited intermediates, HC(OH)=CO* and HCC(OH)=O*, are shown in Figure 2 to illustrate their relative importance. At 49.8 kcal/mol excess energy above the lowest barrier responsible

Table 1
The calculated reaction enthalpies (0 K, in kcal/mol) at the CBS-QB3 level comparing with available experimental values. Numbers in parentheses are 298 K results.

Reactions	This work			Literature[a]
	CBS-QB3	W1U	CBS-APNO	
HCCO + OH → HOCH=C=O **(IM1)**	−87.1(−88.6)	−86.7	−85.5	(−88.6 ± 0.4)
HCCO + OH → 2CO + H_2 **(P1)**	−107.7(−106.4)	−105.9	−105.3	(−104.4 ± 0.5)
HCCO + OH → CO + H_2CO **(P2)**	−105.2(−105.7)	−104.2	−103.2	(−103.9 ± 0.4)
HCCO + OH → CO + ^{1}HCOH **(P3)**	−52.3(−52.7)	−52.0	−50.6	
HCCO + OH → CO_2 + $^1CH_2$ **(P4)**	−44.5(−44.8)	−43.3	−42.2	(−43.1 ± 0.4)
HCCO + OH → CHO + CHO **(P5)**	−32.0(−32.1)	−31.8	−31.4	(−31.3 ± 0.4)
HCCO + OH → H + OCHCO **(P6)**	−16.4(−16.6)	−14.5	−15.0	
HCCO + OH → ^1C_2O + H_2O **(P8)**	0.1(0.0)	0.4	2.1	
HCCO + OH → H + HOCCO **(P9)**	5.2(5.0)	6.0	5.8	
HCCO + OH → CO_2+$^3CH_2$ **(P10)**	−52.4(−52.6)	−52.4	−51.2	(−52.1 ± 0.4)
HCCO + OH → CO + ^{3}HCOH **(P11)**	−26.4(−26.6)	−26.8	−25.6	
HCCO + OH → ^3C_2O + H_2O **(P12)**	−18.9(−18.3)	−18.4	−17.2	(−18.8 ± 0.4)
HCCO + OH → CH_2CO + ^{3}O **(P13)**	−3.1(−3.8)	−3.3	−2.7	(−3.2 ± 0.4)
HCCO + OH → HCCOH + ^{3}O **(P14)**	30.6(30.2)	30.1	31.8	(29.7 ± 0.4)

[a] The data (in kcal mol^{-1}) are derived from literature at 298.15 K: ^{3}O, 58.98 ± 0.02 [37]; OH, 8.92 ± 0.07 [37]; H_2O, −57.80 ± 0.01 [37]; CO, −26.42[38]; CHO, 10.11 ± 0.07 [37]; H_2CO, −25.95[37]; HCCO, 42.61 ± 0.36 [38]; ^3C_2O, 90.55[39]; CH_2CO, −10.64 [37]; HOCH = C = O, −37.08[39]; $^1CH_2$, 102.49 ± 0.38 [37]; $^3CH_2$, 93.50 ± 0.38 [37]; CO_2, −94.04 [39]; HCCOH, 22.27 [39].

Table 2
Comparison of the calculated reaction barriers (at 0 K, in kcal/mol) with the available literature data. Numbers in parentheses are 298 Kvalues.

Reaction	Reaction barrier, $\triangle V^{\neq}$				
	CBS-QB3[a]	W1U[a]	CBS-APNO[a]	G3[b]	CCSD(T)[c]
trans-glyoxal → CO + ^{1}HCOH	60.8(60.9)	60.1	59.6	60.7	–
trans-glyoxal → CO + H_2CO	55.7(55.6)	55.4	54.6	55.4	–
cis-glyoxal → 2CO + H_2	55.6(56.0)	55.8	53.8	55.6	–
trans-HCOH → H_2CO	30.5(30.6)	30.5	29.6	–	29.7
trans-HCOH → *cis*-HCOH	27.1(27.2)	27.1	27.2	27.3	26.8
cis-HCOH → CO + H_2	48.1(48.2)	47.6	46.6	–	47.0

[a] This work.
[b] G3 values from the work of Koch et al. [40].
[c] AE-CCSD(T)/cc-pCVQZ valuesfrom the work of Schreiner et al. [41].

Table 3
Calculated thermochemical parameters of HCCO.

Parameter	CBS-QB3[a]	B3LYP/ 6–311++G(d,p)[b]	G3B3[b]	Exptl. data
ΔH_f (0 K) (kcal/mol)	42.3	43.4	40.7	42.0 ± 0.7 [43]
ΔH_f (298 K) (kcal/mol)	42.6	43.7	41.3	42.2 ± 0.7 [45]
				42.4 ± 2.1 [44]
EA (eV)	2.33	2.31	2.30	2.350 ± 0.022 [44]
IE (eV)	10.83	10.00	10.02	
PA (kcal/mol)	196.7	194.3	197.2	
BDE298 (H–HCCO) (kcal/mol)	106.4	103.4	105.7	105.9 ± 2.1 [44]

[a] This work.
[b] From the work of Hien and coworkers [23].

for the production of CO + HCOH (**P3**), only 3 reactions are seen to be competitive and all others are many orders of magnitude smaller and cannot compete significantly. They are the isomerization of **IM4**–**IM1** by OH migration and **IM4**–**IM5** (oxyiran-2-one) by concerted H-migration and ring formation, and the decarbonylation of **IM1** producing the **P3** product pair. The first two reactions involving **IM4*** was shown to be dominated by the **IM4**–**IM1** conversion as illustrated by a separate Variflex calculation for thermally averaged rate constants by taking into account the structural effects of their transition states. The result indicated that the rate constant for the **IM4**–**IM1** conversion is much greater than that for the isomerization producing **IM5**. Based on this result we can conclude that for the first approximation, the reaction of HCCO + OH via both intermediates produces the CO + HCOH as their primary dominant products. We can therefore predict the rate constant for the reaction on the singlet surface by considering the following processes:

$$OH + HCCO \rightarrow \mathbf{IM1}^* \rightarrow CO + HCOH \quad \text{(Rxn.3)}$$

$$\rightarrow \mathbf{IM4} \rightarrow \mathbf{IM1} \rightarrow CO + HCOH \quad \text{(Rxn.4)}$$

Figure 3 illustrates the individual contributions of the two paths and their total value, which can be represented by

$$k_{P3} = 3.12 \times 10^{-8} T^{-0.59} \exp[-73.0/T] \text{ cm}^3 \text{ molecule}^{-1} \text{ s}^{-1} \times (300 - 2000 \text{ K}) \quad \text{(Eq.4)}$$

At 1000 K, the **IM1** path given by Rxn. 3 contributes 6 times as much **P3** as that from the **IM4** path in Rxn. 4.

3.3.2. Reactions on the triplet surface

As mentioned in the preceding section, the bimolecular reaction of HCOO + OH occurring on the triplet surface produces primarily $^3CH_2 + CO_2$ (**P10**) and ^{3}HCOH + CO (**P11**) as shown in Figure 1b. Variational TST and RRKM calculations have been carried out for following paths with the Variflex code.

$$HCCO + OH \rightarrow IM7^* \rightarrow {}^3CH_2 + CO_2 \ (P10) \quad \text{(Rxn.5)}$$

$$HCCO + OH \rightarrow IM6^* \rightarrow {}^3HCOH + CO \ (P11) \quad \text{(Rxn.6)}$$

As shown in Figure 1b the first reaction occurs via the pre-reaction complex **C2**; the potential energy curve forming **C2** was calculated by lengthening the complexing C–H bond from 2.16 to 5.0 Å

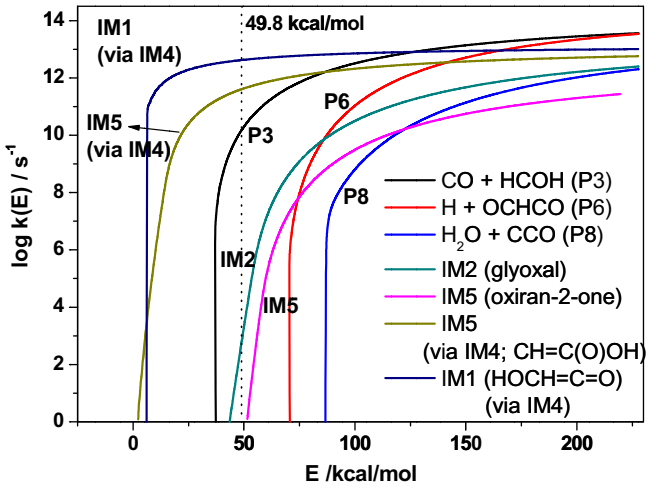

Figure 2. Rate coefficients as a function of energy for the singlet decomposition-channels of HOCH═C═O (**IM1**) and CH═C(O)OH (**IM4**).

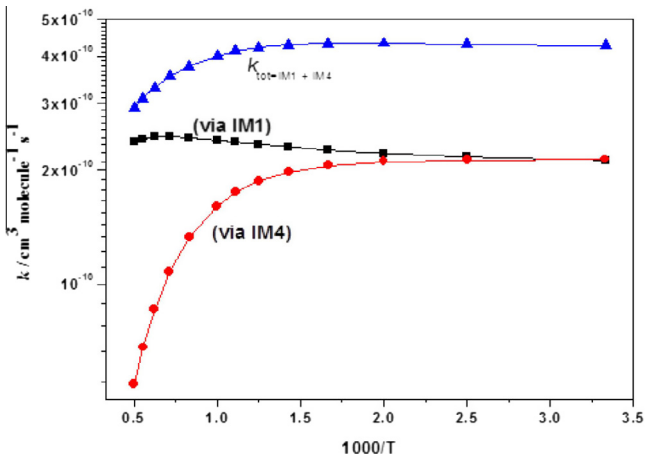

Figure 3. Arrhenius plots of rate constants for production of CO + HCOH via **IM1** and **IM4** in the HCCO + OH reaction.

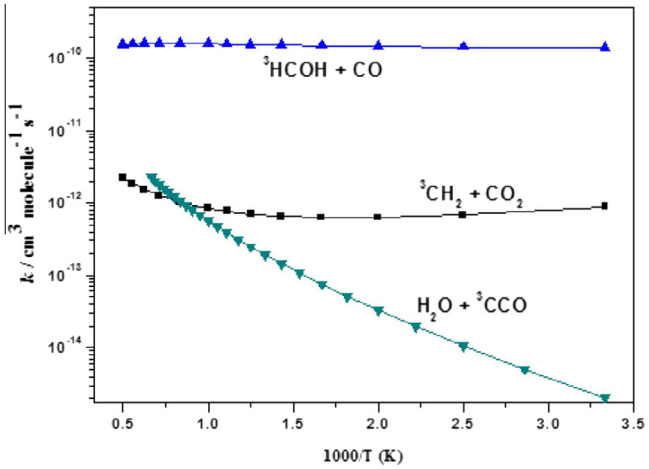

Figure 4. Arrhenius plots of rate constants for HCCO + OH reaction forming various products at triplet surface state at different independent pressures range 0.0001–7600 Torr.

with an interval of 0.1 Å. The computed potential energies can be reasonably fitted to the Morse function with $\beta = 1.33$ Å^{-1}. The rate constants have been predicted for the formation of the $^3CH_2 + CO_2$ products with and without multiple reflections above the **C2** complex. The results indicated that at 300 K (the lowest temperature computed) and at both 760 Torr and the high pressure limit, the effect of multi-reflection corrections is negligible (see Supplementary Figure S2). In addition, the effect of pressure on the $^3CH_2 + CO_2$ (**P10**) product formation is negligible at $P < 7600$ Torr as shown in Figure 4.The predicted rate constant for this process covering the temperature range of 300–2000 K at $P < 7600$ TorrAr pressure can be given by the following three parameter expression:

$$K_{P10} = 1.49 \times 10^{-19} T^{2.09} \exp[1105/T] \text{cm}^3 \text{ molecule}^{-1} s^{-1} \times (300 - 2000\,K) \quad \text{(Eq.5)}$$

The second association reaction of HCCO with OH producing ^{3}HOCHCO (**IM6**) also occurs without a well-defined transition state; the excited IM6 intermediate carries as much as 56.3 kcal/mol of internal energy with 23.1 kcal/mol of excess energy above the transition state for CO elimination via TS13; giving the ^{3}HCOH and CO as shown in Figure 1(b). The computed potential energies of IM6 → HCCO + OH formation by C–O bond breaking could be fitted to the Morse function with $\beta = 3.76$ Å^{-1}. The predicted rate constants at $P < 7600$ TorrAr pressure for ^{3}HCOH + CO (**P11**) formation can be represented in units of s^{-1} by:

$$K_{P11} = 6.29 \times 10^{-11} T^{0.13} \exp[10.8/T] \text{cm}^3 \text{ molecule}^{-1} s^{-1} \times (300\text{—}1000\,K) \quad \text{(Eq.6)}$$
$$4.36 \times 10^{-9} T^{-0.41} \exp[-505.9/T] \text{cm}^3 \text{ molecule}^{-1} s^{-1} \times (1000\text{—}2000\,K)$$

We have also computed the rate constant for the direct H-abstraction reaction, HCCO + OH → H$_2$O + ^{3}CCO which has a 4.1 kcal/mol barrier. As expected, it is much smaller than the complex forming processes discussed above particularly at low temperatures; however, as the temperature increases, it becomes more competitive as shown in Figure 4. The rate constant can be given by the three parameter expression covering the temperature range of 300–2000 K $k_{CCO} = 1.15 \times 10^{-19}\ T^{2.40} \exp(-1186.0/T)$ cm^3 molecule^{-1} s^{-1}. As seen from Figure 4, on the triplet surface the HCCO + OH reaction produces primarily ^{3}HCOH + CO throughout the whole temperature range studied.

4. Concluding remarks

In this work we have carried out a comprehensive computational study on the mechanism for the HCCO + OH reaction using several high-level computational methods including CBS-QB3, CBS-APNO and W1U. The detailed CBS-QB3PES's indicate that the reaction can occur on both singlet and triplet surfaces by OH addition to the C = C Π–bond at both C atoms producing internallyexcited HC(OH)C = O and HCC(OH)=O which can undergo many isomerization and decomposition reactions yielding a variety of intermediates and products, CO + HCOH, $CH_2 + CO_2$, CO + CH_2O, $(HCO)_2$, 2CO + H_2, and other products with high endothermicities. The energy barriers and thermodynamic quantities (such as ΔH_f, ΔH_{rxn}, etc.) for these reactions and the species involved have been computed with the 3 methods and compared with available experimental data. In general, the agreement was found to be excellent. Among the various accessible product channels, the CO + ^{1,3}HCOH products were found to be dominant over the entire temperature range (300–2000 K) studied at $P < 76000$ Torr Ar pressure. Under combustion conditions, the HCOH thus formed can rapidly covert to CH_2O (within a few μs at 1000 K).

To test the validity of the present ab initio chemical kinetic predictive approach by RRKM/ME calculations, we have computed the rate constant for the $(CHO)_2$ decomposition reaction, whose kinetic data are available in the NIST Chemical Kinetics Database (http://kinetics.nist.gov/kinetics/index.jsp). The predicted heats of reaction of glyoxal $(CHO)_2$ and rate constants for dissociation to various products, 2CO + H_2, CH_2O + CO and CHO + CHO, are in good agreement with experimental values as presented in the Supplementary Information.

Acknowledgements

The authors deeply appreciate the support by Taiwan's National Science Council (NSC) under contract No. NSC100-2113-M-009-013 and by the Ministry of Education's ATU program. M.C.L. also acknowledges the support from the NSC for the distinguished visiting professorship at National Chiao Tung University (NCTU) in Hsinchu, Taiwan. L.K.H. would like to thank NSC for the short visit at NCTU in summer 2013. We are also grateful to the National Center for High-performance Computing and Institute for Computational Science and Technology for computer time and the use of its facilities.

Appendix A. Supplementary data

Supplementary data associated with this article can be found, in the online version, at http://dx.doi.org/10.1016/j.cplett.2013.11.060.

References

[1] A.M. Schmoltner, P.M. Chu, Y.T. Lee, J. Chem. Phys. 91 (1989) 5365.
[2] W. Boullart, J. Peeters, J. Phys. Chem. 96 (1992) 9810.
[3] G. Capozza, E. Segoloni, F. Leonori, et al., J. Chem. Phys. 120 (2004) 4557.
[4] T.L. Nguyen, L. Vereecken, J. Peeters, J. Phys. Chem. A 110 (2006) 6696.
[5] S.A. Carl, L. Vereecken, J. Peeters, PCCP 9 (2007) 4071.
[6] G.P. Glass, S.S. Kumaran, J.V. Michael, J. Phys. Chem. A 104 (2000) 8360.
[7] J. Peeters, W. Boullart, K. Devriendt, J. Phys. Chem. 99 (1995) 3583.
[8] J. Peeters, I. Langhans, W. Boullart, et al., J. Phys. Chem. 98 (1994) 11988.
[9] V. Chikan, S.R. Leone, J. Phys. Chem. A 109 (2005) 2525.
[10] S.A. Carl, Q. Sun, J. Peeters, J. Chem. Phys. 114 (2001) 10332.
[11] K.K. Murray, K.G. Unfried, G.P. Glass, et al., Chem. Phys. Lett. 192 (1992) 512.
[12] D.L. Osborn, J. Phys. Chem. A 107 (2003) 3728.
[13] S.J. Klippenstein, J.A. Miller, L.B. Harding, Proc. Combust. Inst. 29 (2002) 1209.
[14] F. Temps, H.G. Wagner, M. Wolf, Z. Phys, Chem. 176 (1992) 27.
[15] S.A. Carl, Q. Sun, L. Teugels, et al., PCCP 5 (2003) 5424.
[16] H.B. Xie, Y.H. Ding, C.C. Sun, J. Phys. Chem. A 110 (2006) 7262.
[17] S.A. Carl, Q. Sun, L. Vereecken, et al., J. Phys. Chem. A 106 (2002) 12242.
[18] J.P. Meyer, J.F. Hershberger, J. Phys. Chem. B 109 (2005) 8363.

[19] K.T. Rim, J.F. Hershberger, J. Phys. Chem. A 104 (2000) 293.
[20] I.V. Tokmakov, L.V. Moskaleva, D.V. Paschenko, et al., J. Phys. Chem. A 107 (2003) 1066.
[21] M.T. Nguyen, W. Boullart, J. Peeters, J. Phys. Chem. 98 (1994) 8030.
[22] J.P. Meyer, J.F. Hershberger, J. Phys. Chem. A 109 (2005) 4772.
[23] M.T. Hien, T.L. Nguyen, S.A. Carl, et al., Chem. Phys. Lett. 416 (2005) 199.
[24] J.X. Zhang, Z.S. Li, J.Y. Liu, et al., J. Phys. Chem. A 110 (2006) 2527.
[25] L. Du, S.A. Carl, Journal of physical chemistry. A 116 (2012) 10074.
[26] J.A. Miller, C.F. Melius, Combust. Flame 91 (1992) 21.
[27] P. Glarborg, M.U. Alzueta, K. Dam-Johansen, et al., Combust. Flame 115 (1998) 1.
[28] M.J. Frisch, G.W. Trucks, H.B. Schlegel, et al., GAUSSIAN 09, Gaussian Inc., Wallingford CT, 2009.
[29] J.A. Montgomery, M.J. Frisch, J.W. Ochterski, G.A. Petersson, J. Chem. Phys. 110 (1999) 2822.
[30] J.W. Ochterski, G.A. Petersson, J.A. Montgomery, J. Chem. Phys. 104 (1996) 2598.
[31] J.M.L. Martin, J. Chem. Phys. 111 (1999) 1843.
[32] P. Celani, H.-J. Werner, J. Chem. Phys. 112 (2000) 5546.
[33] H.-J. Werner, P.J. Knowles, G. Knizia, MOLPRO, Springer, 2010.
[34] S.J. Klippenstein, A.F. Wagner, R.C. Dunbar, et al., Variflex, version 1.0, Argonne National Laboratory, Argonne, IL, 1999.
[35] H. Hippler, J. Chem. Phys. 78 (1983) 6709.
[36] https://www-pls.llnl.gov/data/docs/science_and_technology/chemistry/combustion/prf_tran_dat_v1b.txt.
[37] B. Ruscic, J.E. Boggs, A. Burcat, et al., J. Phys. Chem. Ref. Data 34 (2005) 573.
[38] P.G. Szalay, A. Tajti, J.F. Stanton, Mol. Phys. 103 (2005) 2159.
[39] A. Burcat, B. Ruscic, Argonne National Laboratory, Report (ANL-05/20), Sept. 2005.
[40] D.M. Koch, N.H. Khieu, G.H. Peslherbe, J. Phys. Chem. A 105 (2001) 3598.
[41] P.R. Schreiner, H.P. Reisenauer, Nature 453 (2008) 906.
[42] D.H. Mordaunt, D.L. Osborn, H. Choi, et al., J. Chem. Phys. 105 (1996) 6078.
[43] D.L. Osborn, D.H. Mordaunt, H. Choi, et al., J. Chem. Phys. 106 (1997) 10087.
[44] J.M. Oakes, M.E. Jones, V.M. Bierbaum, et al., J. Phys. Chem. 87 (1983) 4810.
[45] B. Schäfer-Bung, B. Engels, T.R. Taylor, et al., J. Chem. Phys. 115 (2001) 1777.
[46] Y. Ohshima, Y. Endo, J. Mol. Spectrosc. 159 (1993) 458.
[47] L.R. Brock, B. Mischler, E.A. Rohlfing, et al., J. Chem. Phys. 107 (1997) 665.
[48] K.G. Unfrieda, R.F. Curla, J. Mol. Spectrosc. 150 (1991) 86.
[49] K.W. Sattelmeyer, Y. Yamaguchi, H.F. Schaefer, Chem. Phys. Lett. 383 (2004) 266.